

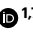


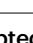
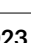





Production vulnerability to wheat blast disease under climate change

Received: 11 August 2022

Accepted: 21 November 2023

Published online: 1 February 2024

 Check for updates

Diego N. L. Pequeno ^{1,7}✉, Thiago B. Ferreira ^{1,2,7}, José M. C. Fernandes ³, Pawan K. Singh ¹, Willingthon Pavan ², Kai Sonder ¹, Richard Robertson ⁴, Timothy J. Krupnik ⁵, Olaf Erenstein ¹ & Senthold Asseng ⁶✉

Wheat blast is a devastating disease caused by the fungal pathogen *Magnaporthe oryzae* pathotype *Triticum* that has spread to both neighbouring and distant countries following its emergence in Brazil in the 1980s. Under climate change conditions, wheat blast is predicted to spread primarily in tropical regions. Here we coupled a wheat crop simulation model with a newly developed wheat blast model, to provide quantitative global estimates of wheat blast vulnerability under current and future climates. Under current climatic conditions, 6.4 million hectares of arable land is potentially vulnerable to wheat blast. A more humid and warmer climate in the future (Representative Concentration Pathway 8.5) is likely to increase the area suitable for wheat blast infection, particularly in the Southern Hemisphere⁵, and reduce global wheat production by 69 million tons per year (13% decrease) by mid-century. Impacts of climate change could be further exacerbated and food security problems increased.

In the 2021–2022 season, wheat was grown on 222 million hectares globally, producing 779 million metric tons of grain¹. Global wheat production is continuously challenged by diseases and pests that are evolving and spreading to new areas as agricultural practices, climate and global trade change. Wheat blast disease caused by the fungal pathogen *Magnaporthe oryzae* pathotype *Triticum* (MoT) has become a substantial threat to wheat production in warm and humid areas². The outbreak of wheat blast currently affecting production was first reported in Brazil in 1985 and then gradually spread to neighbouring countries, causing remarkable yield losses³. In February 2016, the first observation of wheat blast outside South America was recorded in Bangladesh^{4,5}. Shortly after, in 2018, wheat blast was observed for the first time in Zambia⁶. In this study, we simulate the spread and impact of wheat blast disease across continents in current and future climate scenarios, quantifying separately the direct and indirect effects of climate change on wheat production.

Previous yield impact studies have considered the direct effects of climate change from increasing temperatures, precipitation variability

and elevated atmospheric CO₂ concentrations on crop production and have shown that wheat yields in the Southern Hemisphere are likely to be particularly negatively impacted^{7–10}. In this Article, we used the same calibrated wheat simulation model (DSSAT Nwheat) as it is embedded in a global-scale gridded simulation platform for predicting worldwide crop growth and yield¹¹. To integrate the potential effects of wheat blast on yield, a generic disease model (GDM)^{12,13} was parameterized for wheat blast (Extended Data Table 1). The models were coupled at two points. The weather module of DSSAT Nwheat feeds daily information about the environment to the wheat blast model so the density of the fungal spore cloud can be calculated. In turn, the disease damage simulator feeds back information daily to the pest damage modules of DSSAT Nwheat, which updates variables related to leaf, stem, root, seed growth and other plant organs¹². Wheat blast primarily affects the maturing ear but can go on to infect other parts of the plant. Here the damage caused by wheat blast infection was estimated solely on the grain portion of wheat.

¹International Maize and Wheat Improvement Center, Texcoco, Mexico. ²Agricultural and Biological Engineering Department, University of Florida, Gainesville, FL, USA. ³Brazilian Agricultural Research Corporation, Embrapa Trigo, Passo Fundo, Brazil. ⁴International Food Policy Research Institute, Washington, DC, USA. ⁵International Maize and Wheat Improvement Center, Dhaka, Bangladesh. ⁶Technical University Munich, School of Life Sciences, Department of Life Science Engineering, Digital Agriculture, HEF World Agricultural Systems Center, Freising, Germany. ⁷These authors contributed equally: Diego N. L. Pequeno, Thiago B. Ferreira. ✉e-mail: D.PEQUENO@CGIAR.ORG; senthold.asseng@tum.de

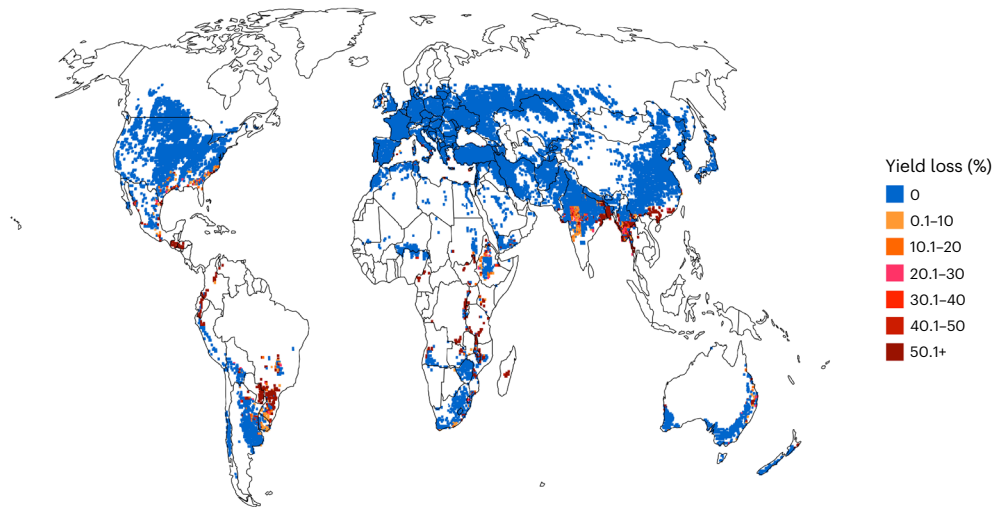


Fig. 1 | Baseline potential wheat yield loss due to wheat blast simulated with climate data from 1980 to 2010. The Decision Support System for Agrotechnology Transfer suite³⁹ with the NWheat crop model⁴⁰ was coupled⁴¹ to

a GDM^{12,13} parametrized for wheat blast, using global input data⁷ in a global-scale gridded simulation platform¹¹. Coloured areas represent the wheat growing areas of the world⁴².

For baseline simulations we used weather data from 1980 to 2010 as input to represent recent conditions⁷. The results show substantial potential yield losses in South America, South Africa and South Asia, which are regions currently affected by wheat blast (Fig. 1). Similar to the reported occurrences of wheat blast in Brazil¹⁴, our simulations show potential for large yield losses in southern Brazil, especially in the State of Paraná. In Bangladesh, the simulated vulnerable regions also coincide well with the main affected regions reported in 2016 (refs. 4–6). In the simulations, districts in southern Bangladesh appear to be most vulnerable, while those in the north, due to cooler and drier weather conditions, have a lower risk for yield loss. A previous study¹⁵ used a climate analogue model (which assumed areas within South Asia with a similar climate as epidemic sites from Bangladesh would be at risk) considering only rainfall, temperatures and humidity. Here, in addition to climate vulnerability, inoculum build-up, spore survival, infection and crop damage were considered. (Extended Data Figs. 1 and 2). We equate vulnerability with the risk of crop losses or failure as a result of biotic factors. More specifically, we define vulnerability as a suite of environmental conditions and host plant presence that favours wheat blast spread, infection and production losses. For Zambia, our model suggests large areas could be vulnerable to the pathogen. An evaluation of the coupled model was performed by simulating the wheat blast outbreaks in Bangladesh and Zambia in 2016 and 2018, respectively, showing that the method was capable of adequately estimating epidemic and non-epidemic years during wheat growing season (Extended Data Fig. 3). Model evaluation was conducted using field collected data for Brazil (Extended Data Fig. 4), Bangladesh and Zambia (Extended Data Fig. 5). Furthermore, field infestation records from Brazil, Bangladesh and Zambia were compared using the confusion matrix approach to our model simulations of disease potential, and the results show the model performed satisfactorily (Extended Data Fig. 6).

Under these historical conditions we found potential for yield loss even in regions where the disease is not yet present. In some countries like Argentina, Zambia and Bangladesh, wheat blast has only been reported in a small portion of the area that could potentially be affected. Other countries or regions like Uruguay, Central America, southeastern USA, East Africa, India and Eastern Australia are currently unaffected but according to our model simulations are vulnerable to wheat blast. Previous studies have detected similar climate suitability for infection in the USA based on The National Centers for

Environmental Prediction Climate Forecast System Reanalysis climate data that are concentrated mainly in the southeast region^{16,17}. By contrast, the risks of wheat blast in Europe and East Asia are low, with close to zero simulated yield loss in their main wheat production areas, except for warm humid areas in southeast China (Fig. 1).

Under climate change scenarios for the period 2040–2070 (Extended Data Table 2), wheat blast is predicted to spread primarily in the tropics and Southern Hemisphere as temperature and relative humidity (RH) increase, resulting in a potential 13% global loss in wheat production annually (Fig. 2). Note that reported yield losses from wheat blast under climate change scenarios consider only the disease impact on yield, excluding percentage yield change due to climate change relative to baseline (equation (11)). A global climate change study using the same DSSAT Nwheat model and input data reported a mean climate change grain yield impact of 1.9% and shows country and regional climate change impact⁷. Country-level and subnational yield data from the Food and Agriculture Organization (FAO) of the United Nations database were not compared in this study due to a lack of methodological clarity in accounting the impacts of pest and diseases in these reports.

In South America, wheat blast could further expand mainly in countries that already suffer losses due to the disease, including Brazil, Argentina, Bolivia and Paraguay⁶. The projections suggest that the presence of wheat blast may also increase in the USA and Mexico, and that the disease may affect previously unaffected countries including Uruguay, Japan, Italy, Spain and New Zealand, among others (Fig. 2). In Africa, countries including Zambia, Ethiopia, Kenya and Congo may suffer from yield losses resulting from the expansion of wheat blast into vulnerable areas. Conversely, under future climates, some parts of India may become less susceptible to wheat blast infection if dry seasonal conditions prevail with more frequent extreme high temperatures (above 35 °C) during the latter part of the wheat growing season. While such high temperatures reduce the likelihood of wheat blast infection, they cause terminal heat stress, reducing overall yield potential¹⁸. Wheat blast may also expand into southeast China, potentially incurring yield losses. Recent studies strongly suggest that *M. oryzae* pathotypes capable of infecting wheat have, in fact, the potential to spread into China with rising temperatures¹⁹.

In Oceania and North America only a small portion of wheat growing area is currently vulnerable to wheat blast, but under climate change this may respectively expand to 5% and 12% of the total wheat area of

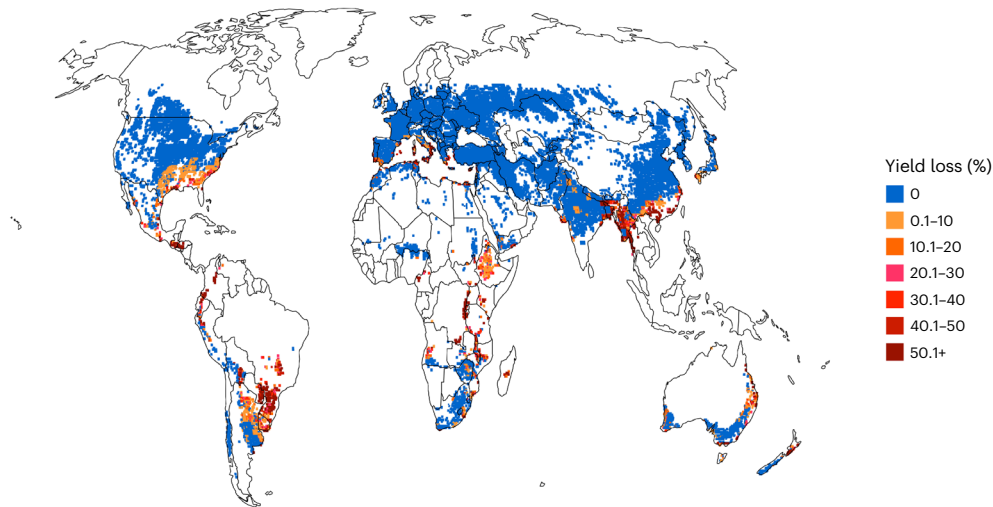


Fig. 2 | Potential wheat yield loss from wheat blast simulated for climate change scenarios for 2040–2070. Representative Concentration Pathway 8.5 simulated with five GCMs was used as input for the Decision Support System for Agrotechnology Transfer suite³⁹ with the NWheat crop model⁴⁰ coupled⁴¹ to the

GDM^{12,13} parametrized for wheat blast, using global input data⁷ in a global-scale gridded simulation platform¹¹. Coloured areas represent the wheat growing areas of the world¹².

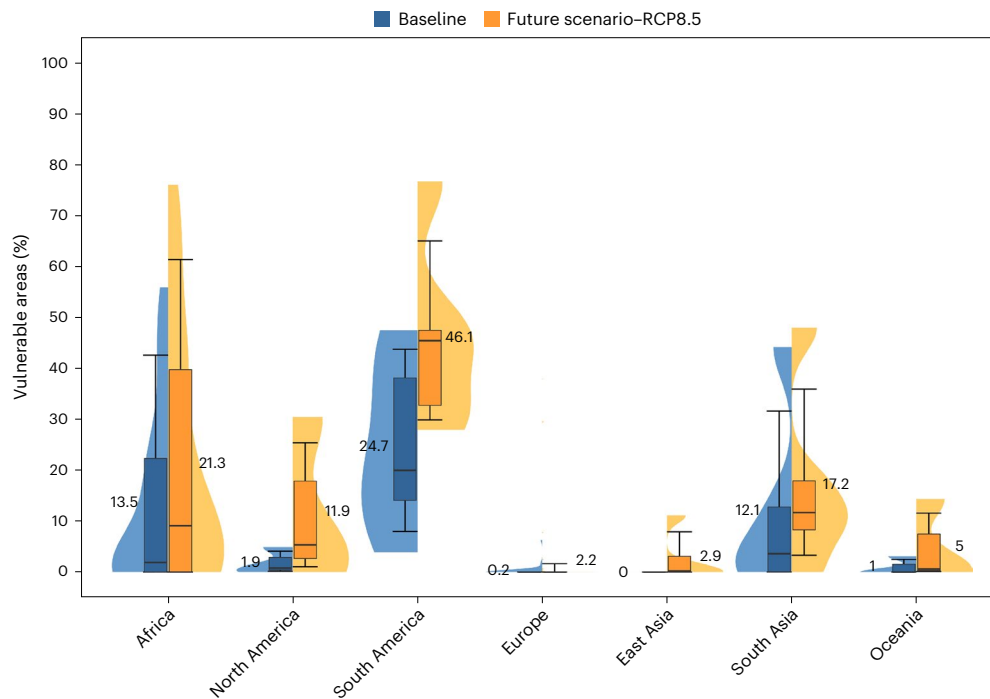


Fig. 3 | Potential continental wheat areas vulnerable to wheat blast damage simulated for the 1980–2010 baseline and for 2040–2070 under climate change. Simulations used historical data for 1980–2010 or the output of five GCMs of Representative Concentration Pathway 8.5 (RCP8.5) for 2040–2070. Boxplots indicate the variability in percentage of wheat growing area per country within continental region that are vulnerable to wheat blast for baseline (blue) and future climate change scenarios (orange) where boxes represent the interquartile range and whiskers extend to the 10th and 90th percentiles. The analysis focused exclusively on nations with wheat growing areas leading to a

total of 33 countries for Africa ($n = 33$), 3 countries for North America ($n = 3$), 5 countries for South America ($n = 5$), 35 countries for Europe ($n = 35$), 4 countries for East Asia ($n = 4$), 4 countries for South Asia ($n = 4$) and 2 countries for Oceania ($n = 2$). Error bars represent differences among countries within the same continental region. Violin plots show the range and relative distribution of variability in disease vulnerability for each continental region. The median of each distribution is shown by the horizontal line in the box, and the mean is given beside each plot. Continental regions are defined in Methods.

these countries (Fig. 3). The cold climate in Europe and other countries where snow falls reduces the chances of survival of the wheat blast spore and thus minimizes the probability of infection (Fig. 3). Although the conditions in the Northern Hemisphere, in general, are not suitable for wheat blast, countries in higher latitudes are affected

by different insect pests and diseases, and climate change will potentially alter their distributions over time²⁰. European regions closer to the Mediterranean may still develop a climate propitious to wheat blast infection, for example, Italy and some parts of southern France and Spain (Fig. 2). Some wheat growing areas in East Asia may also be

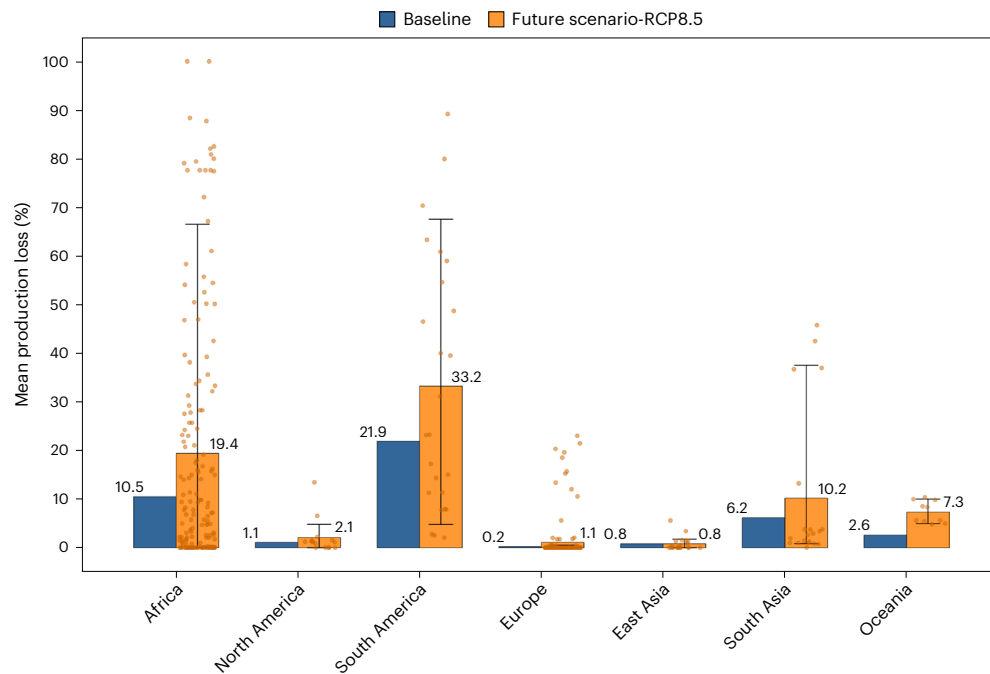


Fig. 4 | Potential mean wheat production loss due to wheat blast damage simulated for the 1980–2010 baseline and for 2040–2070 under climate change. Scenarios were simulated using five GCMs for Representative Concentration Pathway 8.5 (RCP8.5) for 2040–2070 (orange), while historical data were used for 1980–2010 (blue). The direct climate change impact on yield was simulated with and without the modelled potential disease impact to calculate the per cent production loss due to wheat blast alone. Error bars indicate the variability in results among countries in each continental region for

future climate change scenarios using five different GCMs based on the 10th and 90th percentiles. The dot plot corresponds to individual values. The analysis focused exclusively on nations with wheat growing areas with a total of 33 countries for Africa ($n = 165$), 3 countries for North America ($n = 15$), 5 countries for South America ($n = 25$), 35 countries for Europe ($n = 175$), 4 countries for East Asia ($n = 20$), 4 countries for South Asia ($n = 20$) and 2 countries for Oceania ($n = 10$). Continental regions are defined in Methods.

affected by climate change (Fig. 3), with the vulnerability being mostly concentrated in southern China (Fig. 2). The simulations confirmed that the main wheat producing areas vulnerable to wheat blast are in South America, where the disease is already present, and in Africa and South Asia¹⁶ where the pathogen has recently emerged (Fig. 3). It should be noted that the median values for the percentage of vulnerable areas in Fig. 3 are often different from the mean due to uneven distributions that differ for each continental region. The standard error bars are high since we are considering the variability among countries aggregated into these regions. The distribution for South America suggests it will continue to be threatened by wheat blast in the future, and no less than 30% of wheat area would be vulnerable compared with the lower estimated limit of 5% today. The most extreme vulnerability to wheat blast estimated under future climates is in South America and Africa, which may both see up to 75% of wheat areas becoming vulnerable to the disease (Fig. 3).

Simulations of wheat blast in Europe and East Asia show the potential for a small production loss under both scenarios (Fig. 4). If parts of Australia and New Zealand become increasingly susceptible to wheat blast as predicted (Fig. 2), Oceania would experience considerable yield losses (Figs. 2 and 4). As the climate warms southern China and Japan could also become more suitable environments for wheat blast with greater losses expected at harvest than today.

Climate change-induced temperature increase probably contributed to recent wheat blast epidemics such as the 2016 Bangladesh outbreak (Extended Data Figs. 3 and 4) and will drive future occurrences in new countries²¹. The present crop-disease simulation study shows the potential global risk associated with the spread of wheat blast. Wheat blast already threatens 6.4 million hectares under current climatic conditions, which will be further exacerbated by climate change to

13.5 million hectares by mid-century. The increase in vulnerable areas to wheat blast at mid-century is attributed to a combination of rising temperatures and prolonged leaf wetness caused by higher RH (equations (6)–(9)), which create conditions for the pathogen to potentially develop and spread. Such areas are typically concentrated in lower latitudes closer to the Equator, where optimal environmental conditions for wheat blast are more likely to occur. At mid-century, wheat blast alone could reduce global wheat production by 13% (equation (11)). Under these future climatic conditions, South America will be the most affected region, although African and South Asian countries will also be increasingly vulnerable to wheat blast. These areas are noted as some of the most vulnerable areas to the direct impacts of climate change⁷, where food security is already a considerable concern, and wheat consumption is increasing, especially in urban areas²².

Even though previous studies simulated many fungal plant diseases for several crops including wheat, wheat blast is often not considered^{20,23,24}. We conversely show that important global wheat growing areas can be vulnerable and face considerable risks of emerging wheat blast outbreaks beyond Bangladesh and Zambia. In many of these regions, farmers may need to turn to less susceptible crops to mitigate production and financial losses. For example, maize is increasingly grown in former wheat growing areas in Midwest Brazil²⁵. Breeding blast-resistant wheat is a very important strategy⁶ that could mitigate future losses in new vulnerable areas and has already been initiated²⁶. Besides the use of plant breeding and genomic selection to produce wheat varieties resistant to wheat blast, the adjustment in planting date is another effective mitigating strategy against the disease. In regions where the MoT is already present, there is a synchronism between the host and pathogen phenology. During the flowering stage, rain followed by hot and humid weather can promote disease development⁶. To reduce the risk of infection, it is

recommended to avoid early planting in central Brazil and late planting in Bangladesh, as these periods coincide with high temperatures and RH due to increased precipitation levels²⁷. The potential exacerbation of the synchronism between host and pathogen phenology due to climate change highlights the importance of implementing effective mitigation strategies to manage wheat blast. Timely planting to escape conducive wheat blast conditions at the heading stage, combined with other relevant practices, has proven to be effective²⁸.

Moreover, wheat blast itself is changing in a way that may adversely impact wheat production if it overcomes host resistance, gains in virulence and becomes more resistant to fungicide^{4,5}. Several studies have investigated the capability of fungal pathogen adaptation to environmental conditions, which can lead to an increase of virulence and thermal aptitude for infection^{29,30}. A study about the wheat pathogen *Zymoseptoria tritici* has shown a high plasticity and variation in sensitivity to temperature conditions over geographic and seasonal scales within the European-Mediterranean region³¹. The same can also happen with MoT strains, possibly leading to unprecedented yield losses that can exacerbate the pressure on food security and wheat production under the context of climate change.

Although previous research indicates that isolates of the *Triticum* pathotype have the capability for infecting other cultivated crops such as barley, oats and rye and forage grasses^{32,33}, increasing vegetal diversity and crop rotation in agricultural landscape has proven to reduce the impact of fungal diseases^{34,35}. A rice–wheat rotation might serve as an approach to reduce the presence of MoT in the fields since it has been reported that no cross infection could happen between rice and wheat blast isolates³⁶. However, the *Triticum* pathotype population evolves rapidly, leading to a higher level of genetic diversity compared with other pathotypes³⁷. This increased diversity can hinder natural responses against the pathotype, making it more challenging to control³⁸. Vigilance and urgent action are needed to prepare for the increasing wheat blast threat through multiple mitigating strategies including ensuring new cultivars have durable resistance, identifying and implementing integrated disease management practices, and equipping farmers with adequate agronomic practices including adoption of conservation agriculture.

Online content

Any methods, additional references, Nature Portfolio reporting summaries, source data, extended data, supplementary information, acknowledgements, peer review information; details of author contributions and competing interests; and statements of data and code availability are available at <https://doi.org/10.1038/s41558-023-01902-2>.

References

- World agricultural production. USDA <https://apps.fas.usda.gov/psdonline/circulars/production.pdf> (2022).
- Islam, M. T. et al. Wheat blast: a new threat to food security. *Phytopathol. Res.* **2**, 28 (2020).
- Igarashi, R. S. et al. Occurrence of *Pyricularia* sp. in wheat (*Triticum aestivum* L.) in the State of Paraná. *Fitopatol. Bras.* **11**, 351–352 (1986).
- Malaker, P. K. et al. First report of wheat blast caused by *Magnaporthe oryzae* pathotype *Triticum* in Bangladesh. *Plant Dis.* **100**, 2330–2330 (2016).
- Islam, M. T. et al. Emergence of wheat blast in Bangladesh was caused by a South American lineage of *Magnaporthe oryzae*. *BMC Biol.* **14**, 84 (2016).
- Singh, P. K. et al. Wheat blast: a disease spreading by intercontinental jumps and its management strategies. *Front. Plant Sci.* **12**, 1–21 (2021).
- Pequeno, D. N. L. et al. Climate impact and adaptation to heat and drought stress of regional and global wheat production. *Environ. Res. Lett.* <https://doi.org/10.1088/1748-9326/abd970> (2021).
- Rosenzweig, C. et al. Assessing agricultural risks of climate change in the 21st century in a global gridded crop model intercomparison. *Proc. Natl Acad. Sci. USA* **111**, 3268–3273 (2014).
- Jägermeyr, J. et al. Climate impacts on global agriculture emerge earlier in new generation of climate and crop models. *Nat. Food* **2**, 873–885 (2021).
- Asseng, S. et al. Climate change impact and adaptation for wheat protein. *Glob. Chang. Biol.* **25**, 155–173 (2019).
- Robertson, R. Mink: Details of a global gridded crop modeling system. *International Food Policy Research Institute* <https://www.ifpri.org/publication/mink-details-global-gridded-crop-modeling-system> (2017).
- Fernandes J. M. C. et al. in *Advances in Crop Modelling for a Sustainable Agriculture* (ed. Boote, K. J.) Vol. 1, Ch. 5 (Burleigh Dodds, 2019).
- Fernandes J. M. et al. in *Achieving Durable Disease Resistance in Cereals* (ed. Oliver, R.) Vol. 1, Ch. 17 (Burleigh Dodds, 2021).
- Fernandes, J. M. C. et al. A weather-based model for predicting early season inoculum build-up and spike infection by the wheat blast pathogen. *Trop. Plant Pathol.* **42**, 230–237 (2017).
- Mottaleb, K. A. et al. Threat of wheat blast to South Asia's food security: an ex-ante analysis. *PLoS ONE* **13**, 1–15 (2018).
- Duveiller, E. et al. An international perspective on wheat blast. *Phytopathology* **101**, 220 (2011).
- Cruz, C. D. et al. Climate suitability for *Magnaporthe oryzae* *Triticum* pathotype in the United States. *Plant Dis.* **100**, 1979–1987 (2016).
- Arshad, M. et al. Climate variability and yield risk in South Asia's rice–wheat systems: emerging evidence from Pakistan. *Paddy Water Environ.* **15**, 249–261 (2017).
- Shizhen, W. et al. The risk of wheat blast in rice–wheat co-planting regions in China: MoO strains of *Pyricularia oryzae* cause typical symptom and host reaction on both wheat leaves and spikes. *Phytopathology* **111**, 1393–1400 (2021).
- Chaloner, T. M., Gurr, S. J. & Bebber, D. P. Plant pathogen infection risk tracks global crop yields under climate change. *Nat. Clim. Change* **11**, 710–715 (2021).
- Islam, M. T., Kim, K. H. & Choi, J. Wheat blast in Bangladesh: the current situation and future impacts. *Plant Pathol. J.* **35**, 1–10 (2019).
- Mason, N. M., Jayne, T. S. & Shiferaw, B. Africa's rising demand for wheat: trends, drivers, and policy implications. *Dev. Policy Rev.* **33**, 581–613 (2015).
- Bregaglio, S., Donatelli, M. & Confalonieri, R. Fungal infections of rice, wheat, and grape in Europe in 2030–2050. *Agron. Sustain. Dev.* **33**, 767–776 (2013).
- Caubel, J. et al. Climate change effects on leaf rust of wheat: implementing a coupled crop-disease model in a French regional application. *Eur. J. Agron.* **90**, 53–66 (2017).
- Ceresini, P. C. et al. Wheat blast: past, present, and future. *Annu. Rev. Phytopathol.* **56**, 427–456 (2018).
- Wang, S. et al. A new resistance gene in combination with Rmg8 confers strong resistance against triticum isolates of *Pyricularia oryzae* in a common wheat landrace. *Phytopathology* **108**, 1299–1306 (2018).
- Kohli, M. M. et al. in *Wheat Blast* (ed. Kumar, S.) Vol. 1, Ch. 10 (CRC Press, 2020).
- Ascari, J. P. et al. Sequential post-heading applications for controlling wheat blast: a 9-year summary of fungicide performance in Brazil. *Plant Dis.* **105**, 4051–4059 (2021).
- Mariette, N. et al. Local adaptation to temperature in populations and clonal lineages of the Irish potato famine pathogen *Phytophthora infestans*. *Ecol. Evol.* **6**, 6320–6331 (2016).
- de Vallavieille-Pope, C. et al. Thermal generalist behaviour of invasive *Puccinia striiformis* f. sp. *tritici* strains under current and future climate conditions. *Plant Pathol.* **67**, 1307–1320 (2018).

31. Boixel, A. L. et al. Patterns of thermal adaptation in a globally distributed plant pathogen: local diversity and plasticity reveal two-tier dynamics. *Ecol. Evol.* **12**, e8515 (2022).
32. Sharma, R. K. & Singh, P. K. in *Wheat Blast* (ed. Kumar, S.) Vol. 1, Ch. 1 (CRC Press, 2020).
33. Chávez, A. R. et al. Further progress on wheat blast epidemiology: Identification of novel alternate hosts of *Magnaporthe oryzae* *Triticum* pathotype in Paraguay. *Eur. J. Plant Pathol.* **164**, 365–373 (2022).
34. Vialatte, A. et al. in *Advances in Ecological Research* (ed. Bohan, D.A. and Dumbrell, A.) Vol. 65, 133–165 (Academic Press, 2021).
35. Beillouin, D. et al. Positive but variable effects of crop diversification on biodiversity and ecosystem services. *Glob. Change Biol.* **27**, 4697–4710 (2021).
36. Prabhu, A. S. et al. Pathogenic variation among isolates of *Pyricularia oryzae* affecting rice, wheat, and grasses in Brazil. *Int. J. Pest Manag.* **38**, 367–371 (1992).
37. Castroagudín, V. L. et al. Resistance to QoI fungicides is widespread in Brazilian populations of the wheat blast pathogen *Magnaporthe oryzae*. *Phytopathology* **105**, 284–294 (2015).
38. Maciel, J. L. N. et al. Population structure and pathotype diversity of the wheat blast pathogen *Magnaporthe oryzae* 25 years after its emergence in Brazil. *Phytopathology* **104**, 95–107 (2014).
39. Hoogenboom, G. et al. in *Advances in Crop Modelling for a Sustainable Agriculture* (ed. Boote, K. J.) Vol. 1, Ch. 7 (Burleigh Dodds, 2019).
40. Kassie, B. T., Asseng, S., Porter, C. H. & Royce, F. S. Performance of DSSAT-Nwheat across a wide range of current and future growing conditions. *Eur. J. Agron.* **81**, 27–36 (2016).
41. Ferreira, T. B. et al. Coupling a pest and disease damage module with CSM-NWheat: a wheat crop simulation model. *Trans. ASABE* **64**, 2061–2071 (2021).
42. Global spatially-disaggregated crop production statistics data for 2010 Version 1.0. *International Food Policy Research Institute* <https://www.ifpri.org/publication/global-spatially-disaggregated-crop-production-statistics-data-2010-version-10> (2017).

Publisher's note Springer Nature remains neutral with regard to jurisdictional claims in published maps and institutional affiliations.

Open Access This article is licensed under a Creative Commons Attribution 4.0 International License, which permits use, sharing, adaptation, distribution and reproduction in any medium or format, as long as you give appropriate credit to the original author(s) and the source, provide a link to the Creative Commons license, and indicate if changes were made. The images or other third party material in this article are included in the article's Creative Commons license, unless indicated otherwise in a credit line to the material. If material is not included in the article's Creative Commons license and your intended use is not permitted by statutory regulation or exceeds the permitted use, you will need to obtain permission directly from the copyright holder. To view a copy of this license, visit <http://creativecommons.org/licenses/by/4.0/>.

© The Author(s) 2024

Methods

Crop and disease simulation models

DSSAT Nwheat model. The wheat simulation model used in this study was the Nwheat model⁴⁰, part of the Decision Support System for Agrotechnology Transfer, DSSAT v.4.8.0.12 (ref. 39) (Extended Data Fig. 1). The selected wheat model has been widely tested and used to study diverse cropping systems around the world⁴⁰ and was recently connected with pest coupling points⁴¹ designed for linking the wheat model with pest and disease models. The DSSAT Nwheat crop simulation model is embedded within the Mink system, which is a global-scale gridded simulation platform for the use of crop and economic models for agriculture at a global scale¹¹ being calibrated and evaluated for assessment of wheat yield and production under current and future climates⁷.

GDM

The GDM^{12,13} can be parameterized to simulate multiple diseases in several crops. Weather-driven epidemiological models traditionally evaluate infection risk on the basis of climate conditions and consider the inoculum availability according to their specific requirements^{23,43,44}. Studies using this modelling approach led to insightful conclusions that strengthen the association between MoT infection and RH⁴⁵. However, alternate hosts (grasses) in the landscape can serve as potential reservoirs for the inoculum outside the wheat growing season^{33,46,47}. Thus, spore production is more than just dependent on seasonal climate conditions⁴⁸. However, to consider seasonal variability, regional daily weather data were used in our study. The GDM model considers this and simulates the early season inoculum build-up by considering the presence of alternative hosts in the surrounding area before the wheat grain filling stage¹⁴. Daily inoculum dynamics, including spore density in a 1 m³ volume over the crop canopy, survivability and infection, are simulated in a mechanistic way to determine the establishment of the disease and predict wheat blast damage rates during grain-filling stage¹³ (Extended Data Fig. 2). Consequently, simulated locations with suitable in-season climate conditions but with a high density of inoculum during the flowering to the grain-filling stage will result in infection and damage on grain formation and filling⁴⁸.

The DSSAT Nwheat model was coupled⁴¹ with the GDM^{12,13} parameterized for wheat blast using a monolithic approach and global input data⁷. The communication between the GDM and DSSAT Nwheat model occurs in a daily step through coupling points⁴¹ that can affect and reduce state and rate variables such as leaf, stem, root, seed growth and other plant organs progress according to the type of disease infection and damage¹². The DSSAT Nwheat model is the only wheat model publicly available on DSSAT source code with pest coupling points that allow the connection with disease models to estimate biotic damage⁴¹. A similar coupling approach has been created using the STICS wheat model to simulate leaf rust of wheat and estimate the climate change effects on disease dynamics²⁴. However, no coupled process-based model had been parameterized so far to estimate wheat blast and quantify yield loss due to infection. The GDM requires several input parameters related to crop growth, senescence and environmental conditions implemented in the DSSAT-CSM PEST subroutine (Extended Data Figs. 1 and 2).

The GDM was structured following the principles for coupling host and disease dynamics¹³. The disease dynamics were handled at cohort level⁴⁹. The model was designed to represent in detail the disease progress and mimic the disease life cycle. When simulating wheat blast disease, the daily grain mass from the simulated crop growth is regarded as an individual cohort and assumed as a potential infection spot. The disease onset is the result of airborne initial inoculum locally or externally produced. Each cohort represents the crop development on a given day and was used as input for the disease model to estimate sporulation, lesion development and, finally, the total wheat blast impact on the crop on the specific day. The days favouring infection are determined using a combination of conditional rulesets. The model receives as input the cardinal maximum, minimum and optimal

temperatures to calculate the temperature favourability during an infection period. For wheat blast, 35 °C was considered as the maximum temperature, 15 °C as the minimum temperature and 28 °C as the optimal temperature for infection. Daily RH above 90% was deemed favourable to wheat blast infection as water vapour will begin to condense into water droplets over the plant surface⁵⁰. The wheat blast model utilizes a RH threshold that, when exceeded for a minimum duration of 8 h in a single day, triggers the simulation of fungus development. A trapezoidal function, based on cohort age, is used to simulate spore production efficiency and estimated for each cohort the sporulation amount in proportion to the infected lesions (Extended Data Table 1). The presence of alternative hosts in the landscape was considered to predict inoculum build-up during the months preceding spike emergence¹⁴. For each year and each grid cell, the spore cloud simulation commences 60 days before the planting date, assuming the presence of a virtual bondless area with alternate hosts in which the pathogen could infect and initiate the inoculum build-up.

Furthermore, with respect to precipitation, light rainfall (less than 5 mm) is considered desirable for MoT host infection. However, intense rainfalls (above 15 mm) can cause run-off of MoT conidia in sporulating lesions and the freshly deposited spores on leaves and wheat spikes^{48,51}. Thus, when the daily precipitation is above 15 mm, days favouring infection is set to be non-favourable for MoT. The ultraviolet light reduces spore survivability⁵², and the effects were considered according to the difference between the daily maximum and minimum temperature. High values of the difference indicate clear days, while low values indicate cloudy days that favour the longevity of spores in the atmosphere. Under favourable environmental conditions, infection takes place forming an invisible lesion. At the end of the latent period, the lesion becomes visible and infectious and enlarges with time. The model starts with an estimation of the initial pustule size after infection. The growth of lesions was determined using a logistic function associated with the number of hours per day with RH exceeding 90%. At the infectious stage, the spores produced are distributed at three scales of spatial hierarchy⁵³. The rate of infection of a potential spot is computed according to ratios of auto deposition. The GDM model then estimates the total diseased area based on the lesion area with non-visible symptoms. A detailed description of the GDM model is given in Extended Data Fig. 2.

Yield loss estimation

Wheat blast infection impacts crop productivity by causing a deficiency in nutrient translocation, which results in bleached spikes and small, shrivelled and deformed grains⁵⁴. To simulate damage caused by the disease, the epidemiological model estimates the daily percentage of kernels infected according to the total infected area calculated by the GDM. Once the simulation reaches the beginning of the grain formation and filling stage and communicates it to the crop model through a pest coupling point via seed-related state variables⁴¹. The daily damage caused by the infection was quantified as follows:

$$\text{SWIDOT} = \text{SWIDOT} + \text{SDWT} \times \left(\frac{\text{PSDD}}{100} \right), \quad (1)$$

where SWIDOT is the daily seed mass damage (g m⁻² per day), SDWT is the daily seed weight (g per plant per day) and PSDD is the daily percentage of seed mass damage (%).

The daily damage reduces the simulated grain weight by

$$\text{GWAD} = \text{GWAD} - \left(\frac{\text{SWIDOT}}{\text{PLTPOP}} \right), \quad (2)$$

where GWAD is the daily grain weight per plant (g per plant per day) and PLTPOP is plant population (plants m⁻²), which have an impact on simulated grain number estimated as

$$GPP = GPP - GPP \times \frac{\left(\frac{SWIDOT}{PLTPOP}\right)}{GWAD}, \quad (3)$$

where GPP is the daily grain number per plant (g per plant per day).

The impact of the fungal infection also reflects on the grain nitrogen, which further reduces grain development.

$$WTNSD = WTNSD - WTNSD \times \frac{\left(\frac{SWIDOT}{PLTPOP}\right)}{GWAD}, \quad (4)$$

where WTNSD is the daily weight of nitrogen in seed part (g m⁻² per day).

Rising temperatures and changes in precipitation patterns can create a more favourable environment for the fungus to grow and thrive on wheat and other plant species. This allows the inoculum to build up in an area, increasing the risk of wheat infection during grain development. Additionally, increased carbon dioxide levels in the atmosphere are likely to increase the growth and reproduction of the fungus, further exacerbating the problem⁵⁵.

Although wheat blast is mainly considered a wheat spike disease that restricts the development of grains, the pathogen infection can also occur on all other above-ground parts of the plant with various impacts on crop physiology depending on which organs are infected. For example, MoT can interfere with plant growth and photosynthesis before flowering, leading to poor kernel development or even seed abortion later in the growing season⁵⁶. However, the disease model used in this study accounts only for pathogen infection on the wheat spikes. Therefore, the production loss in susceptible areas may potentially be greater than suggested in this study.

Climate data

One of the required variables for simulating wheat blast is RH. The global gridded weather data set from AgEra5 (ref. 57) was uploaded into the CIMMYT high-performance computing cluster that included hourly dewpoint (Dew, K) and temperature (T , K). For each point and with these variables, the RH was calculated through

$$RH = 100 \times \left(\frac{e^{\left(\frac{17.625 \times Dew}{243.04 + Dew}\right)}}{e^{\left(\frac{17.625 \times T}{243.04 + T}\right)}} \right), \quad (5)$$

where RH is hourly RH, Dew is hourly dewpoint and T is hourly temperature.

After estimating the hourly RH, the threshold of 90% was considered as favourable for wheat blast infection because at that humidity level water droplets form on the plant surface⁵⁰. With this threshold, the data were summarized into the daily total number of hours with RH >90% (RH90, input required for the disease model). While it is possible that irrigation methods can create a more humid microclimate that is conducive to the growth and spread of the MoT, irrigation was not considered as a factor for the disease occurrence and spread in our study. A total of 66,880 files (69 GB), each file containing weather information for a point in the global grid (0.5 × 0.5 resolution), were updated with the RH data for a total of 30 years. The updated data set contains data from 1980 to 2010 for the baseline simulations⁷.

The years 1980–2010 were selected as the historical baseline⁷. Daily maximum temperature (T_{max}) and minimum temperature (T_{min}), rainfall and solar radiation were collected from National Centers for Environmental Prediction and University Corporation for Atmospheric Research (NCEP/NCAR) re-analysis database⁵⁸. The spatial resolution of the NCEP data for T_{max} and T_{min} , and solar radiation was approximately 1.884° N/S and 1.865° E/W. Rainfall data at 0.5° resolution corresponding to the same time period was collected from the Global Precipitation Climatological Center of the National Oceanic and Atmospheric Administration.

For the future scenarios (2041–2070), Representative Concentration Pathways 8.5, which represents the highest greenhouse gas

emission scenario, was selected⁷. In total, five global climate models (GCMs) were considered for simulating the future scenarios: (1) US Geophysical Fluid Dynamics Laboratory, (2) The Institute Pierre Simon Laplace, (3) UK Hadley Centre for Climate Prediction and Research, (4) Japan Agency for Marine-Earth Science and Technology, and (5) The Norwegian Climate Centre⁷ (Extended Data Table 2). The baseline and climate change period were chosen in order to simulate 30 years as a standard representation of temporal and spatial climate variability⁵⁹. Additionally, AgMIP has been using this approach as standard, which makes our results also comparable with many other AgMIP studies⁸.

Since future climate change data lacked RH information, the RH was calculated on the basis of daily maximum and minimum temperature. First, the hourly temperature was estimated through a sinusoidal function utilized by DSSAT CSM-CROPGRO model for calculating the effect of temperature on the development of legumes crops in hourly steps³⁹. Then, the dewpoint point was estimated through the daily temperature.

$$Dew_d = (-0.036 \times T_{mean}) + (0.9679 \times T_{min}) + 0.0072 \times (T_{max} - T_{min}) + 1.0111, \quad (6)$$

where Dew_d is daily dewpoint, T_{mean} is daily mean temperature, T_{min} is daily minimum temperature and T_{max} is daily maximum temperature.

This assumption allowed us to estimate the saturated vapour pressure⁶⁰,

$$E_s = 6.11 \times 10^{\left(\frac{7.5 \times T}{237.7 + T}\right)}, \quad (7)$$

where E_s is hourly saturated vapour pressure, the actual vapour pressure⁶⁰

$$E = 6.11 \times 10^{\left(\frac{7.5 \times Dew}{237.7 + Dew}\right)}, \quad (8)$$

where E is hourly vapour pressure, and then calculate the hourly RH

$$RH = \left(\frac{E}{E_s}\right) \times 100. \quad (9)$$

This approach was compared with the RH data used for the baseline for multiple locations (Londrina, Brazil; Obregon, Mexico; Jashore, Bangladesh; and Mpika, Zambia) to assess the accuracy of the resulting data. The RH calculated from temperature was, overall, a reasonable projection compared to the AgERA5 data (Extended Data Fig. 3). This method supplied estimates in the absence of hourly RH data from the GCMs, but could add additional uncertainty to the overall analysis. The daily number of hours with humidity above 90% was extracted and transformed into input for the wheat blast model.

Global crop and disease simulations

For baseline and climatic change scenarios, inoculum was assumed to be uniformly present in all wheat growing areas at the beginning of each growing season, then according to the environmental conditions the GDM model simulates spore survival, infection and damage (Extended Data Fig. 2). All gridded crop modelling simulations were run in the CIMMYT high-performance computer cluster. Two global baseline simulations (1980–2010) were performed, one with disease damage and another without disease damage, to calculate percentage loss due to wheat blast. Ten global climate change simulations were performed, considering all five GCMs (Extended Data Table 1) with disease damage and without disease damage to calculate percentage loss due to wheat blast.

Data processing

Locations with minimum temperature below 12 °C and those with maximum temperature above 37 °C for more than 105 consecutive days were not included as risk areas^{14,17,61}. Areas with a total precipitation

lower than 50 mm for 105 consecutive days before the sowing date were also not included as risk areas as climate conditions were considered too dry for wheat blast development.

Raster files corresponding to each mega-environment cultivar, nitrogen level, sowing dates and GCMs were combined in one single raster, keeping separated irrigated and rainfed simulations. The irrigated and rainfed grain yields were weighted according to the proportion of their areas in the same grid cell^{7,42} using CIMMYT mega-environment cultivar distribution⁶² at $0.5 \times 0.5^\circ$ pixels. Simulated yields are based on representative varieties appropriate for each location and reflect the balance of irrigated and rainfed production⁷. While it is true that irrigation can create a humid environment that is conducive to the growth and spread of the MoT, it should be noted that this factor was not accounted for by the disease model.

For baseline, the yield reduction was expressed as percentage loss by

$$\left(1 - \frac{Y_d}{Y_{nd}}\right) \times 100, \quad (10)$$

where Y_d is yield with disease effect and Y_{nd} is yield without disease effect.

For the climate change scenario, yield percentage loss for each of the five GCMs was estimated analogous to baseline. The final result was calculated using the average percentage loss result of the five GCMs.

The vulnerability was computed as the difference between grain yield with disease and without disease effect, where vulnerable areas exhibit $>0.1\%$ decrease in grain yield due to wheat blast⁶³.

Wheat production was calculated by multiplying the average of 30 years of wheat grain yield by the wheat area for each grid cell. The percentage reduction on global wheat production by mid-century was estimated by comparing the simulated baseline wheat production (529 million tons) against the future projection (460 million tons), both under disease effect, assuming the uniform presence of the pathogen and the potential damage in global wheat growing areas, according to the equation below:

$$RGP_d = \frac{(BGP_d - FGP_d)}{BGP_d} \times 100, \quad (11)$$

where RGP_d is potential reduction of global wheat production due to wheat blast, BGP_d is baseline global production affected by wheat blast and FGP_d is future global production affected by wheat blast.

The regions and continents plotted in Figs. 3 and 4 are Africa (all wheat producing countries), North America (Canada, the USA and Mexico), South America (Argentina, Bolivia, Brazil, Paraguay and Uruguay), Europe (all wheat producing countries), East Asia (China, Japan, North Korea and South Korea), South Asia (Bangladesh, Bhutan, India, Nepal and Pakistan) and Oceania (Australia and New Zealand).

Field empirical data on yield loss

Since the wheat blast emergence in Paraná, Brazil, in 1986 (ref. 3), the City of Londrina has reported the presence of the pathogen during both wheat growing season and off-season⁴⁷. To assess model performance in predicting yield loss due to wheat blast, data were obtained from field trials in Londrina, Paraná, Brazil, from 2012, 2014 and 2015 during the wheat growing season^{28,64}. In each experiment, susceptible varieties (MARFIM for 2012 and 2014 experiments and IPR Catuara TM for 2015 experiment) were used under different fungicide regimes. Additionally, an untreated plot was included as a control in each trial. The experiments were sown during the wheat growing season (between early March and early April). For 2014, two sowing dates were implemented, one sown in early March and another in mid-March, to measure the difference in wheat blast incidence between different planting dates. Randomized block design with four replications was conducted for

each trial, and agronomic practices were performed according to the regional recommendations⁶⁵. Once the crop reached maturity, the plots were harvested to obtain yield as well as the disease incidence, measured as proportion of diseased wheat heads. The incidence of wheat blast was measured in all plots, including those with fungicide applications. Note that even the most efficient fungicide is not able to completely prevent wheat blast infection⁶. It has been reported that the frequency of pathogen mutation has increased³⁷, making it more difficult to assess wheat blast yield loss in field trials.

For simulating these experiments, hourly weather data for all three years were obtained from a weather station in Londrina, Paraná, Brazil ($23^\circ 21' 36.0''$ S, $51^\circ 09' 36.0''$ W) of the Meteorological System of Paraná State (SIMEPAR) and soil profile data of the region were obtained from the Rural Development Institute of Parana (IAPAR). For both wheat varieties, the DSSAT genetic coefficients were estimated on the basis of the reported yield, planting and heading date. The anthesis date was estimated to be 5 days after the reported wheat heading date and was also used for cultivar calibration. Although all fungicide-treated plots reported losses due to wheat blast infection, for each experiment, the highest yield observed between the treated plots was used as a reference for calibrating the cultivars with no disease while the untreated plots were used for the diseased simulations. Since cultivar calibration, in general, depends heavily on the data inputs, the data affected by pests and diseases are not ideal as they will wrongly attribute lower yield potential, for example, to the genotype-specific coefficients of the cultivar when it was due to biotic stress. This undesirable effect on the cultivar parameters is likely to result in biased simulations under different conditions⁶⁶. This method was used strictly to assess the yield loss predictions of the coupled model against empirical data.

The field trial data indicate an inverse correlation between yield and wheat blast incidence. The coupled model simulated grain yields for the untreated plots with an R^2 of 0.86, root mean square error of 95 kg ha^{-1} and Wilmott index of agreement of 0.69 (Extended Data Fig. 4). This indicates that the model could estimate accurately yield loss due to wheat blast infection. The field plots that received fungicide applications obtained greater grain yields compared with the untreated plots. The reported pathogen incidence within fungicide-treated plots ranged from 17.9% to 68.2% (refs. 28,64). The estimated yield loss was 55.7% in 2012, 48.9% for crop sown in early March 2014, 74.7% for crop sown in mid-March 2014, and 68% in 2015. These yield loss percentages were within the yield loss observed on the field in the fungicide trials. Overall, this indicates a good model performance for estimating yield loss from wheat blast disease impact.

Regional wheat blast modelling evaluation

Hourly climate data collected by a weather station near Jashore, Bangladesh ($23^\circ 04' 59.8''$ N, $88^\circ 55' 49.9''$ E), the closest location to the primary areas in which wheat blast was observed during the first outbreak of wheat blast in Bangladesh in 2016, from 2015 to 2020 were used to test if the coupled model was capable of adequately simulating epidemic and non-epidemic years during a wheat growing season (mid-November to early March). AgEra5 weather data were added from the end of 2010 to 2015 to analyse if the antecedent years also had suitable conditions for wheat blast if the inoculum was present earlier. Additionally, using the historical data from 1980 to 2010 for Jashore, the in-season average temperature ($^\circ\text{C}$) from 1980 to 2020 was analysed to see if temperature had overall increased during a 40-year timespan. The same approach was repeated for Mpika, Zambia using the baseline (1980–2010) and AgEra5 data (2010–2020) to analyse the crop growing season (late November to mid-March) in this region (Extended Data Fig. 5).

For Jashore in Bangladesh, the model captured a more consequential loss during the 2015/2016 season, which corresponds to first recorded wheat blast outbreak in Bangladesh⁵. Additionally, the model adequately simulated the following years, which did not report large losses due to wheat blast, especially in 2017/2018, a non-epidemic

year¹³. A recent study used field data to show that the relationship between incidence and damage is not linear, what resulted in very low to zero damage when low incidence of wheat blast was correlated with grain yield damage⁶⁷. The in-season average minimum temperature indicates a notable increase on the temperature compared with the previous years of 17.8 °C between 2015 and 2016 growing season, favouring wheat blast infection. Based on the re-analysis data, throughout the 40-year period, the simulations indicate an in-season average minimum temperature that was constantly above 16.4 °C presenting environmental conditions suitable for wheat blast. For every year, from 2010 to 2020, the results show simulated yield losses ranging from 16.4% to 22.8%. Consequently, the region did not experience a recorded wheat blast outbreak earlier than the 2015/2016 season most probably due to the lack of MoT inoculum in the area.

The simulated potential wheat yield loss for the baseline was compared with confirmed regional reports and research articles from Brazil, Bangladesh and Zambia. The model performance was assessed using a confusion matrix (Extended Data Fig. 6) to classify the results in four categories: (1) regions that were correctly classified as wheat blast vulnerable areas (true positives), (2) regions correctly classified as not vulnerable areas (true negatives), (3) regions that have not reported wheat blast occurrence but the model simulated damage (false positives or type I error) and (4) regions that were reported as wheat blast vulnerable areas but the model did not simulate damage (false negatives or type II error). The unit of measurement considered was the occurrence or not of field infestation records at the state level (Brazil), major administrative divisions (Bangladesh) and provinces (Zambia). The sample size was defined in a binary category of not present, when there is no historical record of wheat blast, or present, when there was at least one wheat blast scouting report in any given year.

Four types of metrics were utilized as classification measures to better analyse the model performance: accuracy, precision, recall and F1 score. Accuracy measures the number of correct predictions using the formula

$$\text{Accuracy} = \frac{\text{TP} + \text{TN}}{\text{TP} + \text{TN} + \text{FP} + \text{FN}}, \quad (12)$$

where TP is the true positive class value, TN is the true negative class value, FP is the false positive class value and FN is the false negative class value.

The precision measures the proportion of regions where wheat blast occurrence was predicted and that were correctly classified by

$$\text{Precision} = \frac{\text{TP}}{\text{TP} + \text{FP}}. \quad (13)$$

Recall identifies the sensitivity of the model in identifying the regions that reported crop loss due wheat blast by

$$\text{Recall} = \frac{\text{TP}}{\text{TP} + \text{FN}}. \quad (14)$$

F1 score uses the harmonic mean of precision and recall measuring the model accuracy by

$$\text{F1 score} = 2 \times \left(\frac{(\text{Recall} \times \text{Precision})}{(\text{Recall} + \text{Precision})} \right). \quad (15)$$

The model simulations have accuracy of 82%, precision of 83%, recall of 94% and F1 score of 88% (Extended Data Fig. 6).

Reporting summary

Further information on research design is available in the Nature Portfolio Reporting Summary linked to this article.

Data availability

The data used and code generated by this study are available at <https://github.com/thiagoferreira53/GlobalWB> (ref. 68). Source data are provided with this paper.

Code availability

The open source code of the Decision Support System for Agrotechnology Transfer (DSSAT) is available at <https://github.com/DSSAT/dssat-csm-os> (ref. 69). The Mink system was designed for High Performance Computing cluster, and the source code is available upon request (r.robertson@cgiar.org). The GDM coupled with DSSAT and the customized computer codes written in R language for data visualization and Python for data collection and processing are available at <https://github.com/thiagoferreira53/GlobalWB> (ref. 68).

References

- Magarey, R. D., Sutton, T. B. & Thayer, C. L. A simple generic infection model for foliar fungal plant pathogens. *Phytopathology* **95**, 92–100 (2005).
- Launay, M. et al. Robustness of crop disease response to climate change signal under modeling uncertainties. *Agric. Syst.* **178**, 102733 (2020).
- Montes, C., Hussain, S. & Krupnik, T. J. Variable climate suitability for wheat blast (*Magnaporthe oryzae* pathotype *Triticum*) in Asia: results from a continental-scale modeling approach. *Int. J. Biometeorol.* **66**, 2237 (2022).
- Lewis, C. M. et al. Potential for re-emergence of wheat stem rust in the United Kingdom. *Commun. Biol.* **1**, 13 (2018).
- Vicentini, S. N. C. et al. Aerobiology of the wheat blast pathogen: inoculum monitoring and detection of fungicide resistant alleles. *Agronomy* **13**, 1238 (2023).
- Danelli, A. L. D. et al. Monitoring *Pyricularia* sp. airborne inoculum in Passo Fundo, Rio Grande do Sul, Brazil. *Summa Phytopathol.* **45**, 361–367 (2019).
- Berger, R. D. et al. A simulation model to describe epidemics of rust of phaseolus beans I. Development of the model and sensitivity analysis. *Phytopathology* **85**, 715–721 (1995).
- Sentelhas, P. C. et al. Suitability of relative humidity as an estimator of leaf wetness duration. *Agric. Meteorol.* **148**, 392–400 (2008).
- Kim C. K. in *Rice Blast Disease* (eds. Zeigler, R. S., Leong, S. A., & Teng, P. S.) 451–464 (CAB International, 1994).
- Li, X. et al. Effects of UV-B radiation on the infectivity of: *Magnaporthe oryzae* and rice disease-resistant physiology in Yuan yang terraces. *Photochem. Photobiol. Sci.* **17**, 8–17 (2018).
- Willcoquet, L. & Savary, S. An epidemiological simulation model with three scales of spatial hierarchy. *Phytopathology* **94**, 883–891 (2004).
- Cruz, C. D. & Valent, B. Wheat blast disease: danger on the move. *Trop. Plant Pathol.* **42**, 210–222 (2017).
- Bencze, S. et al. Response of wheat fungal diseases to elevated atmospheric CO₂ level. *Cereal Res. Commun.* **41**, 409–419 (2013).
- Urashima, A. S. et al. in *Advances in Genetics, Genomics and Control of Rice Blast Disease* (ed. Wang, G.) 267–277 (Springer, 2009).
- Hersbach, H. et al. ERA5 hourly data on single levels from 1959 to present. *Copernicus* <https://cds.climate.copernicus.eu/cdsapp#!/dataset/reanalysis-era5-single-levels> (2018).
- Kalnay, E. et al. The NCEP/NCAR 40-Year Reanalysis Project. *Bull. Amer. Meteor. Soc.* **77**, 437–472 (1996).
- State of the global climate 2020. *World Meteorological Organization* https://library.wmo.int/doc_num.php?explnum_id=10618 (2021).
- Dalezios, N. R., Loukas, A. & Bampzelis, D. Assessment of NDVI and agrometeorological indices for major crops in central Greece. *Phys. Chem. Earth* **27**, 1025–1029 (2002).

61. Cardoso, C. A. et al. Development of a warning system for wheat blast caused by *Pyricularia grisea*. *Summa Phytopathol.* **34**, 216–221 (2008).
62. Sonder, K. Global map of wheat mega-environments. *CIMMYT* <https://hdl.handle.net/11529/10625> (2016).
63. Mottaleb, K. et al. Quantifying wheat blast disease induced yield and production losses of wheat: a quasi-natural experiment. *J. Agric. Appl. Econ.* **55**, 34–56 (2023).
64. Eficiência de fungicidas para controle de brusone de trigo: resultados dos ensaios cooperativos - safra 2015. *Embrapa* <https://ainfo.cnptia.embrapa.br/digital/bitstream/item/159868/1/ID44064-2016CT369.pdf> (2016).
65. Comissão Brasileira de Pesquisa de Trigo e Triticale. Informações Técnicas para Trigo e Triticale. *Embrapa* <https://ainfo.cnptia.embrapa.br/digital/bitstream/item/214730/1/informacoes-tecnicasparatrigoeatricalesafra2020-1592946148.pdf> (2020).
66. Hunt, L. A. & Boote, K. J. in *Understanding Options for Agricultural Production* (ed. Tsuji, G. Y.) (1998).
67. dos Santos, G. B., de Oliveira Coelho, M. A. & Del Ponte, E. M. Critical-point yield loss models based on incidence and severity of wheat head blast epidemics in the Brazilian Cerrado. *Eur. J. Plant Pathol.* **165**, 421–431 (2023).
68. Pequeno, D. N. L. et al. Supporting data for ‘Production vulnerability to wheat blast disease under climate change’. *GitHub* <https://github.com/thiagoferreira53/GlobalWB> (2023).
69. Pequeno, D. N. L. et al. Supporting data for ‘Production vulnerability to wheat blast disease under climate change’. *GitHub* <https://github.com/DSSAT/dssat-csm-os> (2023).
70. Pavan, W., Vargas, F., Perondi, D. & Fernandes, J. M. C. Pic-a-Wheat Field. *Pic-a-Wheat Field* <http://picawheatfield.org/site/#/> (2022).
71. Riaz, M. Effects of wheat genotype, time after inoculation, and leaf age on conidia production by *Drechslera tritici-repentis*. *Phytopathology* **81**, 1298 (1991).
72. Mehta, Y. R. & Zadoks, J. C. Uredospore production and sporulation period of *Puccinia recondita etriticina* on primary leaves of wheat. *Neth. J. Plant Pathol.* **76**, 267–276 (1970).
73. Li, Y. *Factors Influencing the Development of Gray Leaf Spot of Perennial Ryegrass Turf and Seasonal Availability of the Inoculum*. PhD thesis, Pennsylvania State Univ. (2013).
74. Deacon, J. W. in *Fungal Biology* (ed. Deacon, J. W.) (2005).
75. Oneto, L. et al. Timing of fungal spore release dictates survival during atmospheric transport. *Proc. Natl Acad. Sci. USA* **117**, 5134–5143 (2020).
76. Evans, C. K. et al. Inoculum density and infection efficiency of conidia and conidiophores of isolates of *Pyrenophora tritici-repentis*. *Plant Dis.* **80**, 505–512 (1996).
77. Kirtphaiboon, S. et al. Model of rice blast disease under tropical climate conditions. *Chaos Solitons Fractals* **143**, 110530 (2021).
78. Précigout, P. A. et al. Does the latent period of leaf fungal pathogens reflect their trophic type? A meta-analysis of biotrophs, hemibiotrophs, and necrotrophs. *Phytopathology* **110**, 345–361 (2020).
79. Mills, K. B. et al. Quantifying the effects of temperature and relative humidity on the development of wheat blast incited by the *Lolium* pathotype of *Magnaporthe oryzae*. *Plant Dis.* **104**, 2622–2633 (2020).
80. Sah, D. N. Effects of leaf wetness duration and inoculum level on resistance of wheat genotypes to *Pyrenophora tritici-repentis*. *J. Phytopathol.* **142**, 324–330 (1994).
81. Geagea et al. Dry-dispersal and rain-splash of brown (*Puccinia recondita* f. sp. *tritici*) and yellow (*P. striiformis*) rust spores from infected wheat leaves exposed to simulated raindrops. *Plant Pathol.* **48**, 472–482 (1999).
82. Rajput, L. S. et al. Effect of temperature on growth and sporulation of rice leaf blast pathogen *Magnaporthe oryzae*. *Int. J. Curr. Microbiol. Appl. Sci.* **6**, 394–401 (2017).
83. Suzuki, H. Studies on the behavior of the rice blast fungus spore and application to outbreak forecast of rice blast disease. *Bull. Hokuriku Natl Agric. Exp. Stn.* **10**, 1–118 (1969).
84. Suzuki, H. Meteorological factors in the epidemiology of rice blast. *Ann. Rev. Phytopathol.* **13**, 239–256 (1975).
85. Monitoring *Pyricularia* sp. airborne inoculum in Passo Fundo, Rio Grande do Sul, Brazil. *Summa Phytopathol.* **45**, 361–367 (2020).

Acknowledgements

S.A., D.N.L.P., P.K.S. and T.B.F. were supported by the CGIAR research programme on Wheat Agri-food systems (CRP WHEAT). P.K.S., D.N.L.P. and T.B.F. received support from the One CGIAR Plant Health Initiative (PHI) and the One CGIAR Foresight Initiative provided support for D.N.L.P., K.S. and R.R. T.J.K. and J.M.C.F. were supported by the Transforming Agrifood Systems in South Asia (TAFSSA), and by the USAID and Bill and Melinda Gates Supported Cereal Systems Initiative for South Asia (CSISA). P.K.S. and S.A. acknowledge support of the Agriculture Model Intercomparison and Improvement Project AgMIP, and P.K.S. of the Australian Centre for International Agriculture Research (ACIAR). T.J.K. acknowledges support of the Bill & Melinda Gates Foundation [INV-029117]. Under the grant conditions of the Foundation, a Creative Commons Attribution 4.0 Generic License has already been assigned to the Author Accepted Manuscript version that might arise from this submission. We thank all funders who supported CGIAR Research Initiatives through their contributions to the CGIAR Trust Fund (<https://www.cgiar.org/funders/>). The views expressed here are those of the authors and do not necessarily reflect the views of the funders or associated institutions.

Author contributions

S.A., W.P. and D.N.L.P. conceptualized the paper. Data curation was carried by T.B.F., D.N.L.P., K.S. and T.J.K. and the formal analysis by T.B.F. and D.N.L.P. The methodology was conceived by S.A., T.B.F., D.N.L.P., J.M.C.F., P.K.S. and W.P., and the validation was carried out by D.N.L.P., T.B.F., J.M.C.F., P.K.S. and T.J.K. T.B.F., D.N.L.P. and R.R. conducted the software implementation and T.B.F. and K.S. the visualization. The manuscript was written originally by T.B.F., D.N.L.P. and S.A. and reviewed and edited by T.B.F., D.N.L.P., S.A., O.E., P.K.S., T.J.K., J.M.C.F., W.P., K.S. and R.R.

Competing interests

The authors declare no competing interests.

Additional information

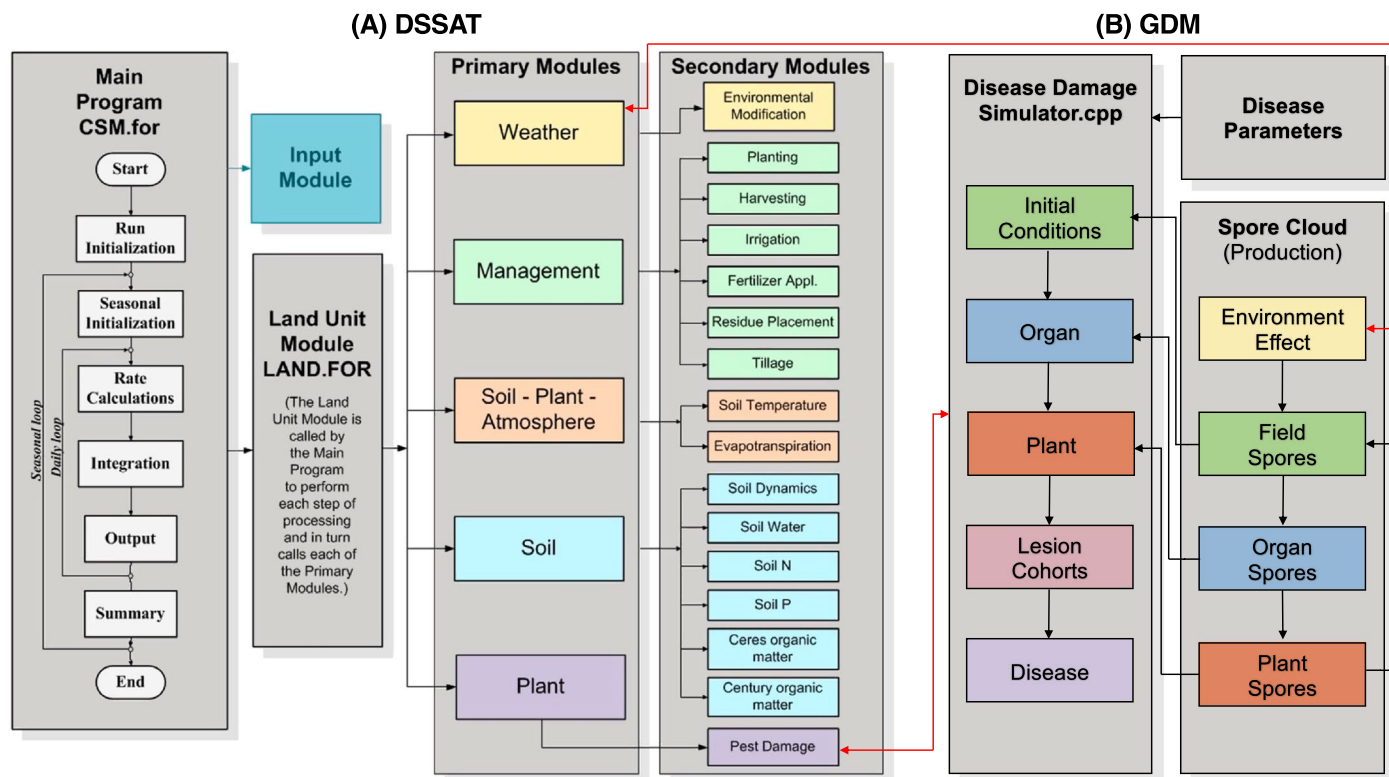
Extended data is available for this paper at <https://doi.org/10.1038/s41558-023-01902-2>.

Supplementary information The online version contains supplementary material available at <https://doi.org/10.1038/s41558-023-01902-2>.

Correspondence and requests for materials should be addressed to Diego N. L. Pequeno or Senthold Asseng.

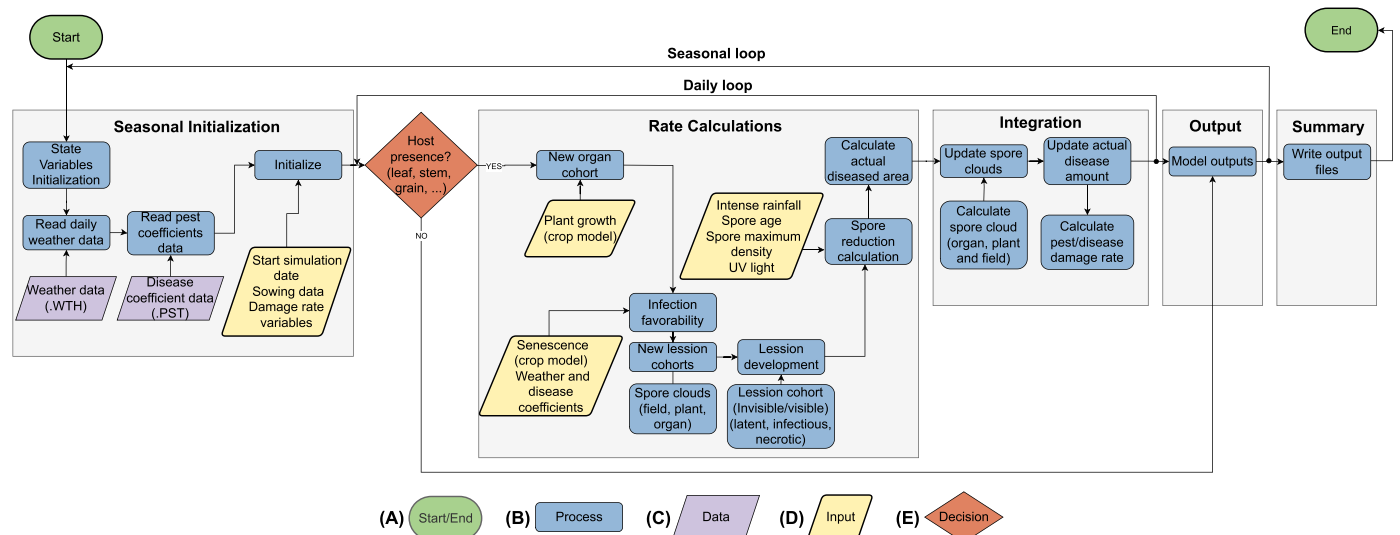
Peer review information *Nature Climate Change* thanks Tofazzal Islam, Maria Lodovica Gullino, Marie Launay and the other, anonymous, reviewer(s) for their contribution to the peer review of this work.

Reprints and permissions information is available at www.nature.com/reprints.



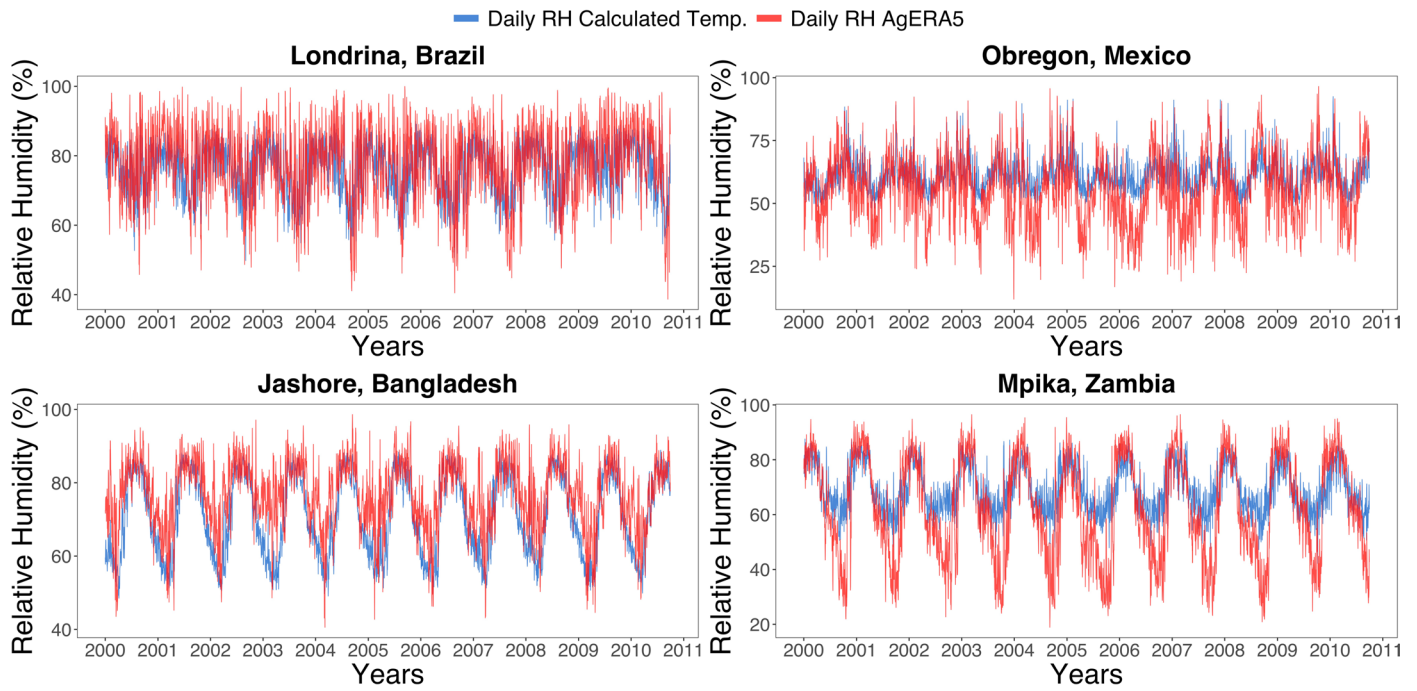
Extended Data Fig. 1 | The structure of the Decision Support System for Agrotechnology Transfer, DSSAT (A), and the Generic Disease Model, GDM (B). The red lines show how DSSAT and GDM models exchange information and simulate disease damage. The GDM model uses weather data from DSSAT and specific disease parameters as input to estimate the daily spore production and cloud density. It simulates the spores in the field and on the plant organs based

on weather conditions, even when there is no infection. Whenever there are appropriate conditions for disease infection and host plant is present, the GDM model simulates in daily steps the disease life cycle and returns to the wheat model the respective damage at the cohort level affecting the plant growth state variables through the DSSAT Pest Damage module.



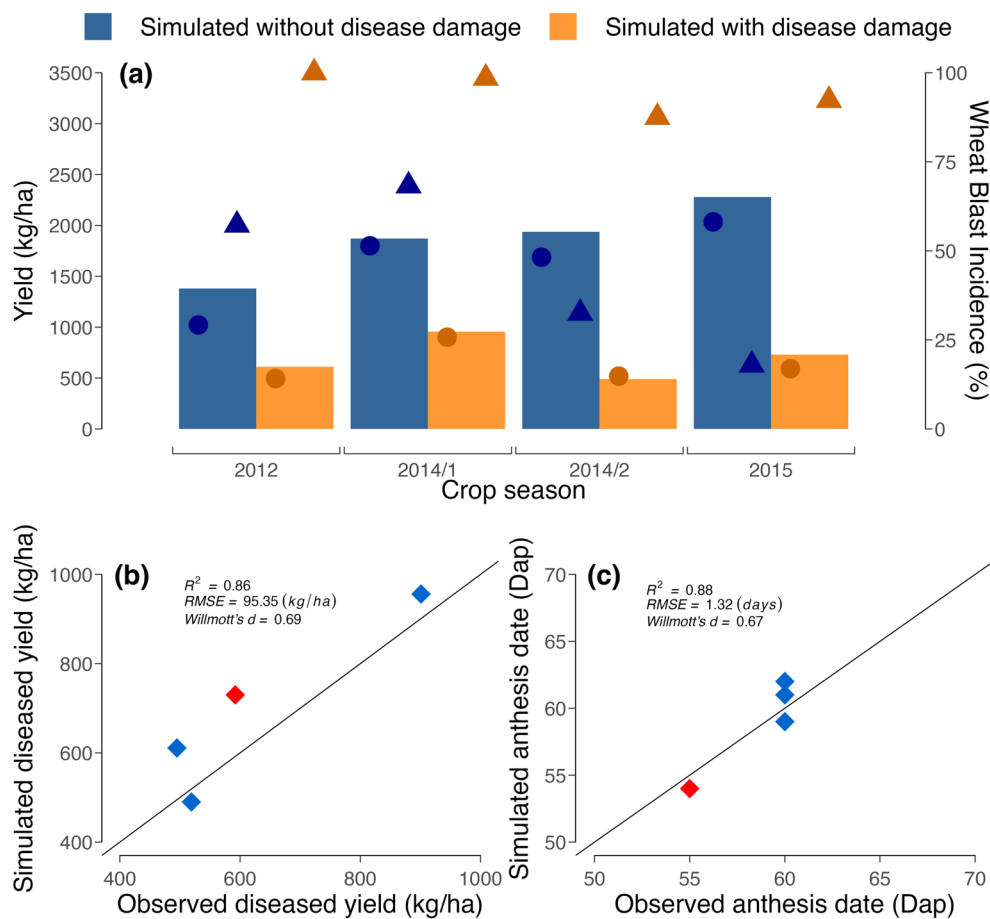
Extended Data Fig. 2 | Diagram of the Generic Disease Model (GDM). The diagram utilizes flowchart symbols to build the conceptual representation of the model. Start/End (a) indicates the beginning or end of the program. Process (b) represents the functions within the system. Data (c) represents data files and Input (d) represents specific input values that are used by the model. Decision (e) is a decision-making statement based on specific criteria. The GDM model uses a daily-step simulation and follows a specific execution order that matches the one used by the Nwheat model within the Crop System Modeling (CSM) of the DSSAT. Within the Seasonal Initialization, the model initializes the state and damage variables, reads the weather data (.WTH) for estimating wheat blast development based on the disease coefficient data file (.PST) and begin the seasonal simulation. According to the host presence and the daily crop growth, the model estimates the disease progress in the Rate Calculations section. Daily

disease development is managed at cohort level^{12,13}. Each cohort represents the crop development on a given day and was used as input for the disease model to estimate sporulation, lesion development and finally, the total wheat blast impact on the crop on the specific day. For wheat blast, fungal damage is only calculated after seed development stage. During the Rate Calculations, the model calculates the disease process by estimating spore growth within the field, plant and organ (cohorts). Environmental factors such as rain and UV light are considered as limiting factors on spore survivability. In Integration, spore dispersion is estimated according to the dispersal coefficients provided in the disease coefficient data file. The daily disease damage is estimated at this stage and communicated to the crop growth model through the specific damage rate variable that will reduce the development of the plant part affected by the disease.



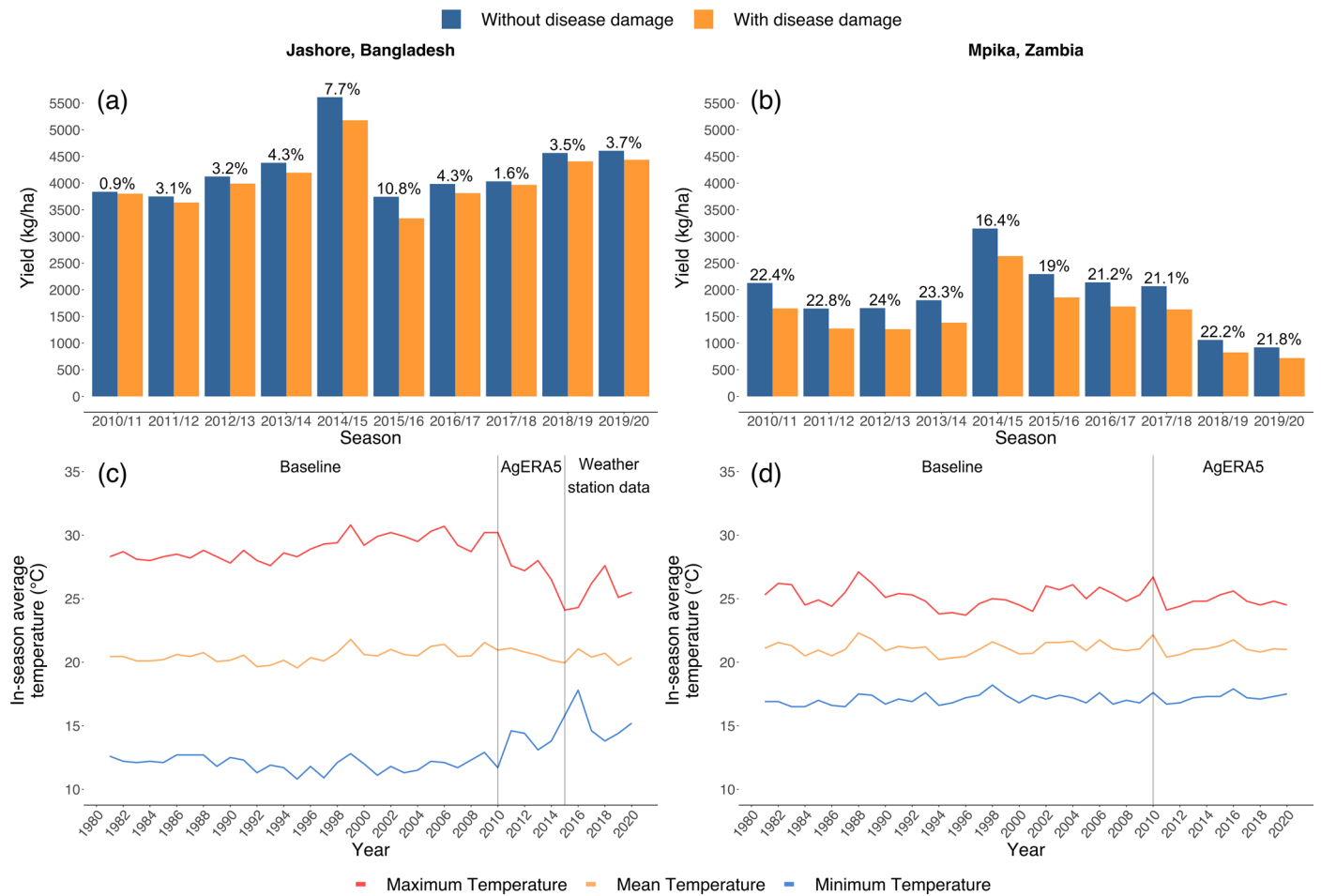
Extended Data Fig. 3 | Daily relative humidity (RH) from AgEra5 compared with the calculated daily relative humidity for four locations with contrasting climate. The line in red indicates the daily RH from AgERA5 while the blue line indicates the calculated daily RH. Daily relative humidity was

calculated using daily maximum and minimum temperatures from the year 2000 to 2010. This comparison was made in four different locations in contrasting regions of the globe (Londrina, Brazil; Obregon, Mexico; Jashore, Bangladesh; and Mpika, Zambia) were used for this analysis.

**Extended Data Fig. 4 | Model evaluation against observed field trial data.**

(a) simulated grain yield without (blue) and with (orange) wheat blast disease damage compared against three years of field collected data from Londrina, Paraná - Brazil. Circles represent the observed yield in fungicide treated plots (dark blue) and untreated plots (dark orange). Triangles represent the observed wheat blast incidence in fungicide treated plots (dark blue) and untreated plots

(dark orange). All field plots, including those under fungicide applications, presented wheat blast incidence. Bottom identity plots comparing simulated untreated plot yield (b) and anthesis date (c) against empirical data (days after planting). Diamond symbol represents the field observed data for the wheat cultivars IPR Catuara TM (light red) and Marfim (light blue).



Extended Data Fig. 5 | Comparison of simulated grain yield without (blue) and with (orange) wheat blast disease damage from 2010 to 2020 and recorded in-season weather data from 1980 to 2020 in Jashore, Bangladesh (left panels), and Mpika, Zambia (right panels). The top graphs (a and b) show simulated grain yield and percent damage for each season from 2010 to 2020.

The bottom graphs (c and d) show crop in-season (from sowing to harvest) average maximum, minimum, and mean temperature from 1980 to 2020 using baseline weather data, AgERA5 and weather station data. The number above each set of two bars shows the additional simulated damage for the disease in %.

		Reported wheat blast damage	
		H_1	H_0
Simulated wheat blast damage	H_1	<p>True Positive Brazil (7) Bangladesh (5) Zambia (3) Total (15)</p>	<p>False Positive Brazil (0) Bangladesh (1) Zambia (2) Total (3)</p>
	H_0	<p>False Negative Brazil (0) Bangladesh (1) Zambia (0) Total (1)</p>	<p>True Negative Brazil (1) Bangladesh (1) Zambia (1) Total (3)</p>

Extended Data Fig. 6 | Confusion matrix showing the model's performance.

This matrix contrasts model simulation areas with wheat blast and actual observed data from Brazil^{6,14,28,70–85}, Bangladesh and Zambia⁶. Field infestation records at the state level (Brazil), major administrative divisions (Bangladesh), and provinces (Zambia) were considered in this comparison. The numbers in parenthesis represent occurrences in each of four categories: true positive (when

the simulations show wheat blast damage and these were confirmed by national reports and research articles); true negative (when the simulations show no disease damage and no disease infection was ever reported); false positive (type I error, when model simulates disease damage but no disease infection was ever reported); and false negative (type II error, when the model simulates no disease damage but wheat blast damage was reported).

Extended Data Table 1 | Coefficients defined in the Generic Disease Model (GDM) for simulating wheat blast dynamics and infection

Variable	Value	Reference
DPSL	1500 (#)	Riaz et al. (1991)
SPE	15,22,28,35 (°C)	Riaz et al. (1991)
SCF	0.98669,10.71894,0.93374	Mehta and Zadoks (1970)
MSCD	15000 (# m ⁻³)	Riaz et al. (1991); Li et al. (2013)
ASR	0.044 (%)	Expert estimate
SPO2P	1	Expert estimate
SPO2F	1	Expert estimate
CCFPO	3,6,9 (# days)	Deacon et al. (2005); Oneto et al. (2020)
II	500 (# m ⁻³)	Expert estimate
TFS	35,15,28 (°C)	Cardoso et al. (2008)
IE	0.8 (%)	Evans et al. (1996); Kirtphaiboon et al. (2021)
IPS	0.001 (cm ²)	Expert estimate
LP	7 (# days)	Précigout et al. (2020); Kirtphaiboon et al. (2021); Mills et al. (2020)
IP	21 (# days)	Kirtphaiboon et al. (2021)
WT	8 (hours day ⁻¹)	Sah (1994)
DRE	$0.367753 \times (r + 0.001)^{0.129605} \times e^{(-0.085252 \times (r + 0.001))}$	Expert estimate
WF	$1/(1 + e^{(4.948 - 0.348 \times r)})$	Cardoso (2008)
IGF	$0.01 + (r \times (0.2/9))$	Geagea (1999)
VGF	$0.0161858 \times e^{(-e^{(1.563509 - 0.441721 \times r)})}$	Rajput et al. (2017)
MRRS	15 (mm)	Suzuki et al. (1969); Suzuki et al. (1975); Danelli (2019)

Model variables include DSPL, Daily Spore Production per Lesion; SPE, Spore Production Efficiency; SCF, Sporulation Crowding Factors; MSCD, Maximum Spore Clouds Density; ASR, Attainable Spore Rate; SPO2P, Spore Proportion that moves from Organ cloud to Plant cloud; SPP2F, Spore Proportion that moves from Plant cloud to Field cloud; CCFPO, Cloud compartmentalization (days till leaving the system - die/remove) (Field, Plant, Organ); II, Initial Inoculum; TFS, Temperature Favorability in the infection period (maximum, minimum and optimal); IE, Infection Efficiency; IPS, Initial Pustule Size; LP, Latent Period; IP, Infection Period; WT, Wetness Threshold; DRE, Dispersion Rain Effect where r stands for daily precipitation (mm); WF, Wetness Factor, where r stands for daily precipitation (mm); IGF, Invisible Growth Function, where r stands for daily precipitation (mm); VGF, Visible Growth Function, where r stands for daily precipitation (mm); and MRRS, Millimeters of rain needed to reduce spores cloud number.

Extended Data Table 2 | Global climate models (GCM) utilized for climate scenario simulations

Climate Model	Model Acronym
US Geophysical Fluid Dynamics Laboratory	GFDL-EM2M
The Institute Pierre Simon Laplace	IPSL-CM5A-LR
UK Hadley Centre for Climate Prediction and Research	HadGEM2-ES
Japan Agency for Marine-Earth Science and technology	MIROC-ESM-CHEM
The Norwegian Climate Centre	NorESM1-M

The simulations were conducted using global daily weather data projections from the US Geophysical Fluid Dynamics Laboratory (GFDL-EM2M), The Institute Pierre Simon Laplace (IPSL-CM5A-LR), UK Hadley Centre for Climate Prediction and Research (HadGEM2-ES), Japan Agency for Marine-Earth Science and technology (MIROC-ESM-CHEM) and The Norwegian Climate Centre (NorESM1-M).

Reporting Summary

Nature Portfolio wishes to improve the reproducibility of the work that we publish. This form provides structure for consistency and transparency in reporting. For further information on Nature Portfolio policies, see our [Editorial Policies](#) and the [Editorial Policy Checklist](#).

Statistics

For all statistical analyses, confirm that the following items are present in the figure legend, table legend, main text, or Methods section.

- | n/a | Confirmed |
|-------------------------------------|--|
| <input type="checkbox"/> | <input checked="" type="checkbox"/> The exact sample size (n) for each experimental group/condition, given as a discrete number and unit of measurement |
| <input type="checkbox"/> | <input checked="" type="checkbox"/> A statement on whether measurements were taken from distinct samples or whether the same sample was measured repeatedly |
| <input checked="" type="checkbox"/> | <input type="checkbox"/> The statistical test(s) used AND whether they are one- or two-sided
<i>Only common tests should be described solely by name; describe more complex techniques in the Methods section.</i> |
| <input checked="" type="checkbox"/> | <input type="checkbox"/> A description of all covariates tested |
| <input checked="" type="checkbox"/> | <input type="checkbox"/> A description of any assumptions or corrections, such as tests of normality and adjustment for multiple comparisons |
| <input type="checkbox"/> | <input checked="" type="checkbox"/> A full description of the statistical parameters including central tendency (e.g. means) or other basic estimates (e.g. regression coefficient) AND variation (e.g. standard deviation) or associated estimates of uncertainty (e.g. confidence intervals) |
| <input checked="" type="checkbox"/> | <input type="checkbox"/> For null hypothesis testing, the test statistic (e.g. F , t , r) with confidence intervals, effect sizes, degrees of freedom and P value noted
<i>Give P values as exact values whenever suitable.</i> |
| <input checked="" type="checkbox"/> | <input type="checkbox"/> For Bayesian analysis, information on the choice of priors and Markov chain Monte Carlo settings |
| <input checked="" type="checkbox"/> | <input type="checkbox"/> For hierarchical and complex designs, identification of the appropriate level for tests and full reporting of outcomes |
| <input checked="" type="checkbox"/> | <input type="checkbox"/> Estimates of effect sizes (e.g. Cohen's d , Pearson's r), indicating how they were calculated |

Our web collection on [statistics for biologists](#) contains articles on many of the points above.

Software and code

Policy information about [availability of computer code](#)

- | | |
|-----------------|---|
| Data collection | The data set used is a large scale representation of agricultural systems from many sources and all software used to collect the data are available in github. |
| Data analysis | Software used for the study are the Decision Support System for Agrotechnology Transfer, DSSAT v.4.8.0.12; The Generic Disease Model, GDM, v.1.0; Mink system, a global-scale gridded simulation platform for the use of crop and economic models for agriculture at a global scale; and customized computer codes written in R language for data visualization and Python for data processing. |

For manuscripts utilizing custom algorithms or software that are central to the research but not yet described in published literature, software must be made available to editors and reviewers. We strongly encourage code deposition in a community repository (e.g. GitHub). See the Nature Portfolio [guidelines for submitting code & software](#) for further information.

Data

Policy information about [availability of data](#)

All manuscripts must include a [data availability statement](#). This statement should provide the following information, where applicable:

- Accession codes, unique identifiers, or web links for publicly available datasets
- A description of any restrictions on data availability
- For clinical datasets or third party data, please ensure that the statement adheres to our [policy](#)

The data used and generated by this study are available on Github (<https://github.com/thiagoferreira53/GlobalWB>).

Research involving human participants, their data, or biological material

Policy information about studies with [human participants or human data](#). See also policy information about [sex, gender \(identity/presentation\), and sexual orientation](#) and [race, ethnicity and racism](#).

Reporting on sex and gender	<input type="checkbox"/> Our findings do not apply to reports on sex and gender.
Reporting on race, ethnicity, or other socially relevant groupings	<input type="checkbox"/> Our findings do not apply to reports on human research population.
Population characteristics	<input type="checkbox"/> Our findings do not apply to reports on human research population.
Recruitment	<input type="checkbox"/> No participants were recruited.
Ethics oversight	<input type="checkbox"/> There was no need for approved study protocol.

Note that full information on the approval of the study protocol must also be provided in the manuscript.

Field-specific reporting

Please select the one below that is the best fit for your research. If you are not sure, read the appropriate sections before making your selection.

Life sciences Behavioural & social sciences Ecological, evolutionary & environmental sciences

For a reference copy of the document with all sections, see [nature.com/documents/nr-reporting-summary-flat.pdf](https://www.nature.com/documents/nr-reporting-summary-flat.pdf)

Ecological, evolutionary & environmental sciences study design

All studies must disclose on these points even when the disclosure is negative.

Study description	<input type="checkbox"/> A process-based crop model (DSSAT-NWHEAT) was coupled with a disease model (GDM) to predict where wheat blast disease can spread next and how detrimental it will be to future grain production using five climate models for mid century.
Research sample	<input type="checkbox"/> Wheat blast previous reports from Brazil and Bangladesh were used taking into account past epidemics to test model accuracy and potential to spread in other regions of the globe for current and future scenarios. We used baseline and five global climate models from the Coupled Model Intercomparison Project (CMIP) phase 5 bias-adjusted and downscaled by ISIMIP.
Sampling strategy	<input type="checkbox"/> Previous reports at state level (Brazil), major administrative divisions (Bangladesh), and provinces (Zambia) were considered to test the model accuracy to determine how vulnerable are the areas already affected in the past.
Data collection	<input type="checkbox"/> The wheat blast data was collected from previous studies and national reports. Crop and disease models simulations were providing grain yield, percent damage, and vulnerability for the study.
Timing and spatial scale	<input type="checkbox"/> Crop model simulations run from 1980 to 2010 for baseline and 2040 to 2070 for future scenario at 0.5° of spatial resolution globally.
Data exclusions	<input type="checkbox"/> We excluded from this study areas that do not cultivate wheat using SPAM crop production statistics data (https://www.ifpri.org/publication/global-spatially-disaggregated-crop-production-statistics-data-2010-version-10).
Reproducibility	<input type="checkbox"/> Crop and disease models versions and inputs are described and available to ensure reproducibility.
Randomization	<input type="checkbox"/> Not relevant, data are not grouped for a specific statistical analysis test, only grouped to perform descriptive statistical analysis.
Blinding	<input type="checkbox"/> Not relevant, process-based models and disease models used are independent.
Did the study involve field work?	<input checked="" type="checkbox"/> Yes <input type="checkbox"/> No

Field work, collection and transport

Field conditions	<input type="checkbox"/> Hourly weather data (temperature, precipitation, and solar radiation) for all three years, 2012, 2014, and 2015, were obtained from a weather station in Londrina, Paraná Brazil (23°21'36.0"S 51°09'36.0"W) of the Meteorological System of Paraná State (SIMEPAR). Hourly climate data collected by a weather station near Jashore, Bangladesh (23°04'59.8"N 88°55'49.9"E) from 2015 to 2020 was also used.
Location	<input type="checkbox"/> Londrina, Paraná Brazil (23°21'36.0"S 51°09'36.0"W) and Jashore, Bangladesh (23°04'59.8"N 88°55'49.9"E).

Access & import/export	The data is open access and was obtained from government websites, publications, and web data servers (e.g. Github).
Disturbance	Not relevant.

Reporting for specific materials, systems and methods

We require information from authors about some types of materials, experimental systems and methods used in many studies. Here, indicate whether each material, system or method listed is relevant to your study. If you are not sure if a list item applies to your research, read the appropriate section before selecting a response.

Materials & experimental systems

- | n/a | Involved in the study |
|-------------------------------------|--|
| <input checked="" type="checkbox"/> | <input type="checkbox"/> Antibodies |
| <input checked="" type="checkbox"/> | <input type="checkbox"/> Eukaryotic cell lines |
| <input checked="" type="checkbox"/> | <input type="checkbox"/> Palaeontology and archaeology |
| <input checked="" type="checkbox"/> | <input type="checkbox"/> Animals and other organisms |
| <input checked="" type="checkbox"/> | <input type="checkbox"/> Clinical data |
| <input checked="" type="checkbox"/> | <input type="checkbox"/> Dual use research of concern |
| <input checked="" type="checkbox"/> | <input type="checkbox"/> Plants |

Methods

- | n/a | Involved in the study |
|-------------------------------------|---|
| <input checked="" type="checkbox"/> | <input type="checkbox"/> ChIP-seq |
| <input checked="" type="checkbox"/> | <input type="checkbox"/> Flow cytometry |
| <input checked="" type="checkbox"/> | <input type="checkbox"/> MRI-based neuroimaging |